Controlled boron content in lightly B-doped single crystal diamond films by variation of methane concentration

Peer-reviewed author version

ROUZBAHANI BAYATANI, Rozita; POBEDINSKAS, Paulius; Donatini, Fabrice; Wong, Deniz; Pernot, Julien & HAENEN, Ken (2024) Controlled boron content in lightly B-doped single crystal diamond films by variation of methane concentration. In: CARBON, 221 (Art N° 118923).

DOI: 10.1016/j.carbon.2024.118923
Handle: http://hdl.handle.net/1942/42451

Controlled Boron Content in Lightly B-doped Single Crystal Diamond Films by Variation of Methane Concentration

Rozita Rouzbahani[*1], Paulius Pobedinskas[1], Fabrice Donatini[2], Deniz Wong[3], Julien Pernot[2], and Ken Haenen[*1]

[1]*Institute for Materials Research (IMO), Hasselt University, and IMOMEC, IMEC vzw, Wetenschapspark 1, Diepenbeek, Belgium*

[2]*Université Grenoble-Alps, CNRS, Institut Néel, Grenoble, France*

[3]*Helmholtz-Zentrum Berlin für Materialien und Energie, Hahn-meitner-Platz 1, D-14109 Berlin, Germany*

E-mails: rozita.rouzbahani@uhasselt.be and ken.haenen@uhasselt.be

Abstract

Obtaining desirable electrical properties from B-doped single crystal diamond (SCD) films hinges on precise control of boron incorporation into the crystal lattice structure. In this study, the impact of methane concentration during plasma deposition on boron incorporation of lightly B-doped SCD films is investigated. SCD layers are grown successively by microwave plasma enhanced chemical vapor deposition (CVD) at different methane-to-hydrogen concentrations (1%, 2%, and 3%), with residual boron atoms present in the CVD reactor. An increase in methane concentration leads to surface defects such as unepitaxial crystallites and pyramidal hillocks. The charge carrier mobility, electrical conductivity, and boron content of samples are evaluated and discussed. The temperature-dependent mobility is analyzed through

Corresponding authors. Tel: +3211268847. E-mail: rozita.rouzbahani@uhasselt.be (Rozita Rouzbahani), Tel: +3211268875. E-mail: ken.haenen@uhasselt.be (Ken Haenen)

theoretical modeling, revealing dominant scattering mechanisms at different temperatures. At 300 K, the maximum hole mobility reached 1200 $cm^2/V\cdot s$ for the 1% methane concentration sample, transitioning to hopping conduction at lower temperatures. An increase in boron-doping level with rising methane concentration is detected by Fourier transform infrared spectroscopy, cathodoluminescence spectroscopy, Hall effect, and X-ray photoelectron spectroscopy measurements. These findings highlight the potential of methane concentration in plasma feedgas to control boron concentration in CVD diamond and open avenues for crafting efficient high-power electronic applications using *p*-type SCD films.

Keywords: Boron doped single crystal diamond, methane concentration dependence, residual boron, CVD diamond growth.

Introduction

Boron doped single crystal diamond (SCD) is a well-known candidate material for the next generation power electronic devices, and controlling the boron incorporation in its structure is one of the most laborious challenges. In recent years, the growth of lightly B-doped SCD with boron concentrations below 10^{16} cm^{-3} and hole mobility above 2200 $cm^2/V\cdot s$ have gained attention for the fabrication of high-power diamond Schottky diodes.[1–4] One of the promising method to achieve high crystalline quality of B-doped SCD films is through crystallization from a carbon solution in metal melts at high pressure and high temperature (HPHT). However, it has been observed that synthetic HPHT single crystals of diamond can exhibit various crystal forms with different predominate faces, which strongly depends on the growth conditions such as temperature, pressure, and used metals for catalysis and inhibition.[5,6] Therefore, B-doped HPHT diamonds have a non-uniform distribution of boron, dependent on the growth sector, potentially impacting the performance diamond-based electronic devices.[6,7] On the other hand, microwave plasma enhanced chemical vapor deposition (MW PE CVD) is an appropriate method to have a good control of diamond electrical conductivity by the uniform incorporation of boron atoms in the crystal lattice structure for electronic devices,[8–14] even if it is still a challenge to reach a low boron doping ($< 5 \times 10^{15}$ cm^{-3}).[15] Another crucial factor is the ability of growing a high crystalline quality of B-doped SCD film with a low density of dislocations and surface defects, because several growths are required to resume in order to fabricate the drift layer of electronic devices such as Schottky diodes.[8,11,16,17]

The effect of methane concentration on the crystalline quality of homoepitaxial diamond films has been extensively studied.[8,18–21] A low concentration ratio ($\leq 0.5\%$) of methane-to-hydrogen ($[CH_4]/[H_2]$) in the plasma feedgas mainly resulted in the high crystalline quality of SCD films.[16] However, obtaining the required thickness (a few tens of micrometers) of diamond

56 films needed for power electronics, e.g. vertical Schottky barrier diodes becomes both
57 time-consuming and cost-prohibitive with such a low $[CH_4]/[H_2]$ ratio ($\leq 0.5\%$), primarily due
58 to a low deposition rate (≤ 0.4 μm/h).[22,23] In order to obtain higher growth rates, which reduces
59 the fabrication cost, it is required to increase the methane concentration. Nevertheless, the
60 increase of methane concentration may cause the appearance of several types of surface defects
61 such as unepitaxial crystallites.[8,18,24,25] These defects are known to increase the leakage current
62 and reduce the breakdown field in high power electronic devices, due to the fact that the leakage
63 current is likely to flow through these defects and provide alternative conduction
64 pathways.[16,26,27] Hence, an optimized CVD growth condition is demanded to deposit a SCD
65 layer with a low density of surface defects at reasonably high growth rate.

66 In our previous study,[23] the impact of methane concentration in the plasma feedgas on the
67 electrical properties of heavily boron doped SCD films was investigated. The results revealed
68 that by increasing the methane concentration, the B-doping level in the films was also
69 increased. *Ab initio* density-functional theory calculations showed that the presence of CH_2
70 sites has no significant impact on the binding energy of an adsorbed boron atom. However, the
71 presence of CH_2 sites increases the chance of H-defect site formation, *i.e*. places where the
72 diamond lattice is not terminated with a hydrogen atom, providing additional binding sites for
73 boron. These results have great potential to provide a route to understand impurity
74 incorporation in diamond on a general level, of great importance for doping but also colour
75 center formation.[28]

76 The purpose of the current work is to develop a new protocol allowing coupling methane
77 concentration and boron incorporation to reach lightly B-doped SCD grown layers with an
78 improvement of the surface quality with a low density of surface defects. Along these lines, a
79 series of experiments that varied the methane concentration in the plasma feedgas have been
80 carried out in this study.

Materials and Methods

Unintentionally boron doped diamond was homoepitaxially grown on 3 mm × 3 mm type Ib HPHT SCD substrates provided by Sumitomo Electric. A 2.45 GHz MW PE CVD homemade metal chamber reactor containing a 4.5 cm inside diameter fused silica tube was used for the deposition.[29] The orientation of diamond substrate surfaces was less than 1° off of the (100) crystallographic orientation, as measured by X-ray diffraction. Prior to being loaded into the CVD reactor, diamond substrates were acid cleaned, as described in our previous work.[23] The base pressure in the reactor was ≈ 3×10^{-7} mbar before igniting the hydrogen plasma. A hydrogen plasma treatment was performed on the substrates using a temperature of 800℃, a gas flow of 500 sccm, a microwave power of 315 W, and a pressure of 200 mbar (20 kPa) for approximately 45 min. A new fused silica tube, which was not contaminated by boron, was used for this series of experiments.[30] Unintentionally B-doped diamond films were then grown with 1%, 2%, and 3% of $[CH_4]/[H_2]$ ratios in the plasma feedgas, sequentially. The boron atoms source was related to the memory effect of metal chamber used previously for the growth of heavily B-doped SCD films with trimethylboron. These growths were performed at a pressure of 200 mbar (20 kPa) and a total gas flow of 500 sccm. Microwave power was varied between 315 W and 320 W to maintain a constant substrate temperature at 780–800℃. The temperature was measured every 20 min during the 2 h deposition time by a Minolta/Land Cyclops 52 Infrared Thermometer in the peak measuring mode with emissivity set to 0.6. This pyrometer is designed to operate within wavelength range of 3.4 μm to 3.9 μm, minimizing errors arising from emissivity, ensuring maximum accuracy in temperature measurements. Sample thickness was measured by a Mitutoyo Linear Gage (Model EH-101P) at the center of the sample, avoiding surface defects, nine times and given as an average over all measurements.[23] The grown films were characterized by optical microscopy and atomic force microscopy (AFM) to

identify the main topological defects. AFM scans were performed on a Bruker Multimode 8 in tapping mode. The Fourier transform infrared (FTIR) transmission spectrum was measured by a Bruker Tensor 27 FTIR spectrometer. For each sample, a spectrum of the HPHT diamond substrate was measured prior to growth, and then for the grown diamond layer on the substrate after deposition. Hence, any variation in the transmission spectrum is due to the grown diamond films, signifying that any newly observed absorption feature occurs exclusively within the thickness of the grown layer. Hall effect measurements were carried out in a Transient Signal Technologies vacuum chamber at temperature ranges from 90 K to 700 K using the van der Pauw method.[23] All of the diamond surfaces were chemically oxidized by acid cleaning prior to metal deposition. Four Ti/Au (20 nm/50 nm) Ohmic contacts with a 250 µm diameter were deposited at the corners of the samples by a homemade dual magnetron sputtering system, without breaking the vacuum between the depositions. The Ohmic nature of the contacts was confirmed at several temperatures between 90 K to 700 K by the observation of linear current-voltage characteristics for each contact pair. For cathodoluminescence (CL) spectroscopy, an electron beam generated by a FEI Quanta 200 scanning electron microscopy gun was focused on the sample (0.2-30 kV acceleration voltage) in order to generate electron-hole pairs. The sample was located on a cold stage GATAN using the liquid helium to set the temperature (5 K to 300 K). The detection system was composed of a parabolic mirror collecting the light generated and focusing it on the lens and entrance slit of a Jobin Yvon HR460 monochromator. The monochromator was associated with a photomultiplier or charge coupled device, placed at the exit of the spectrometer, to analyze the emitted light and generate a spectrum. To measure the samples of this study at 5 K, the entrance slit size of monochromator was chosen to be 0.2 mm, and the acceleration voltage was fixed to 30 kV. X-ray photoelectron spectroscopy (XPS) measurements on the diamond samples were performed in the beamline U41-PEAXIS at the BESSY II synchrotron.[31] The XPS analyzer

was a commercial PHOIBOS 150 EP hemispherical analyzer from SPECS.[32] Photoelectrons, emitted from the sample after the photon absorption, were collected by the electron analyzer mounted at the sample chamber. The excitation (1000 eV) and the pass (20 eV for C1s and 100 eV for B1s) energies of the analyzer were kept constant whereas the kinetic energy of the electrons was varied. The energy resolution of the analyzer was constant throughout the scan. During the measurements, the pressure inside the experimental chamber was ≈ 10^{-8} mbar.

Results and Discussion

The homoepitaxial CVD diamond grown film morphologies, observed by optical microscope, are compared in Figure 1. For the sample with 1% methane concentration, a high surface quality was achieved exhibiting very few visible surface defects such as small hillocks and unepitaxial crystallites on the grown surface. When the methane concentration was increased to 2%, the number of unepitaxial crystallite defects (dark dots in Fig. 1) increased, which leads to a degraded surface quality of the film. Moreover, the SCD film grown at 3% methane concentration contains an even higher number of surface defects like unepitaxial crystallites and hillock defects compared to the previous two samples grown at lower methane concentrations (1% and 2%). This can be a consequence of the high growth rate at 3% methane concentration (see Table 1) and/or bad polishing of the as-received HPHT substrate. The latter is proposed due to the appearance of some defects along what appears to be a polishing line (Fig. 1(c)).

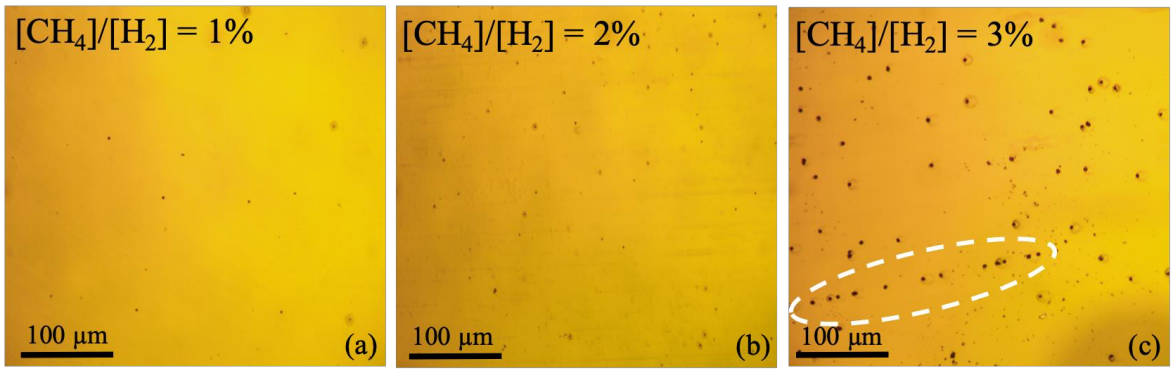

Figure 1: Optical micrographs show the surface morphology of SCD samples grown with: (a) 1%, (b) 2%, and (c) 3% methane concentration in the plasma feedgas. (c) The white dashed oval marks surface defects created along a polishing line.

In order to define the identity of the defects on the sample grown with 3% methane concentration, its surface morphology was investigated by AFM (Fig. 2). Figure 2 shows one of the pyramidal hillocks that consists of four-fold symmetry defects, featuring inclination angles between 3.1° to 5.7°, and truncated by an unepitaxial crystallite on the top. These pyramidal hillocks have sizes up to 30 µm in lateral dimension. Lloret *et al.*[33] reported that high methane concentrations result in the generation of the $\mathbf{b}=\frac{1}{2}<011>$ family of threading dislocations. When it is energetically favourable, in undoped or lightly doped SCD samples, such threading dislocations tend to dissociate into partial $\mathbf{b}=\frac{1}{6}<211>$ Burgers vectors by a Shockley mechanism.[34] This process changes the Burgers vector family and introduces stacking faults which may form micro {111} disoriented planes that favour the generation of penetration twins. In addition to the mechanism governing the formation of such defects, it is believed that hillock formation may arise due to stacking faults or dislocations that originate at the interface between the surface and the CVD grown layer from lattice defects or suboptimal substrate polishing (Fig. 1(c)), or propagate from the substrate into the CVD layer.[35,36] Furthermore, it was reported that these regions consist of agglomerated impurities, primarily composed of Fe, Mo, and amorphous carbon.[36,37] These metals are present as impurities in HPHT substrates, as well as within the growth chamber and substrates holder.

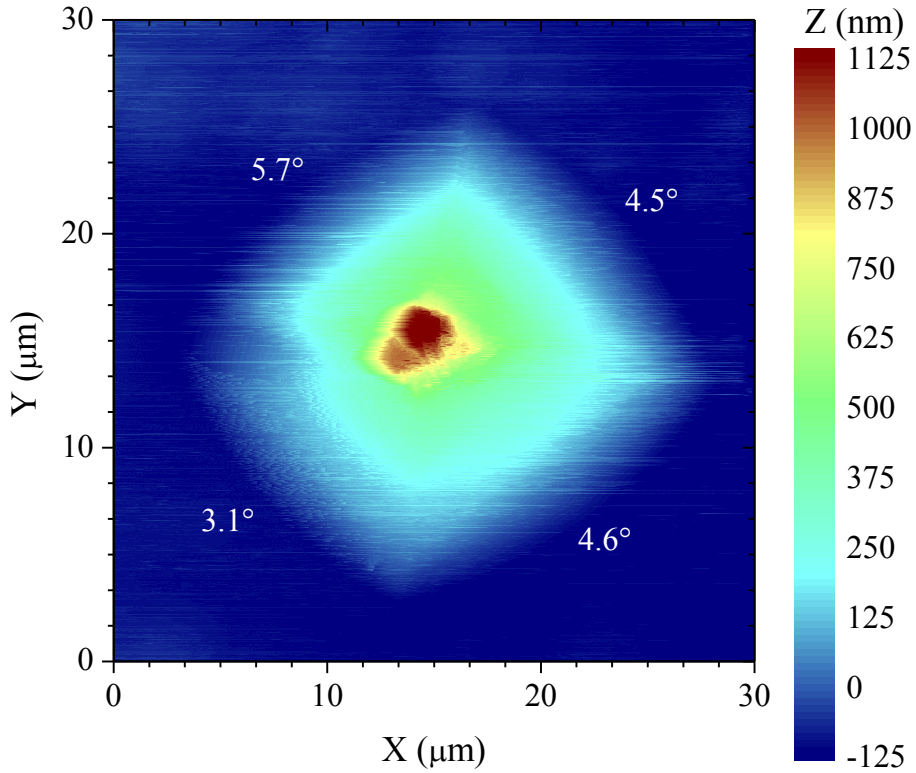

Figure 2: AFM image of a pyramidal hillock exhibiting an unepitaxial crystallite in its centre, observed in the sample grown at 3% methane concentration. The inclination angle of each side of the hillock is also provided.

The analysis of the FTIR transmission spectrum focused on the absorption feature at 2800 cm^{-1} (Fig. 3), which is attributed to the second excited state electronic transition of the neutral boron acceptor.[38,39] This peak has been correlated with the boron content in diamond to estimate doping levels in the range of 10^{16} cm^{-3} to 10^{18} cm^{-3}.[38–41] The uncompensated acceptor concentration ($N_a - N_d$) can be evaluated using the equation given by Collins and Williams for the peak at 2800 cm^{-1}.[42] The inset of Figure 3 shows a plot of absorption coefficient vs. energy, which can give the integrated area of the 2800 cm^{-1} absorption peak, I_{2800}. Fitting a baseline to these data, enables the use of a relationship between I_{2800} and $N_a - N_d$:

$$N_a - N_d = 8 \times 10^{17} I_{2800} \ (\mathrm{cm}^{-3}) \tag{1}$$

The uncompensated acceptor concentrations of films prepared at methane concentrations of 2% and 3% were estimated to be 4.5×10^{17} cm^{-3} and 5.6×10^{17} cm^{-3}, respectively. While the spectrum of the sample with 1% methane concentration has no obvious FTIR peak at

184 2800 cm^{-1}, this simply demonstrates a SCD film without visible evidence of a boron

185 incorporation higher than 10^{16} cm^{-3}.[42]

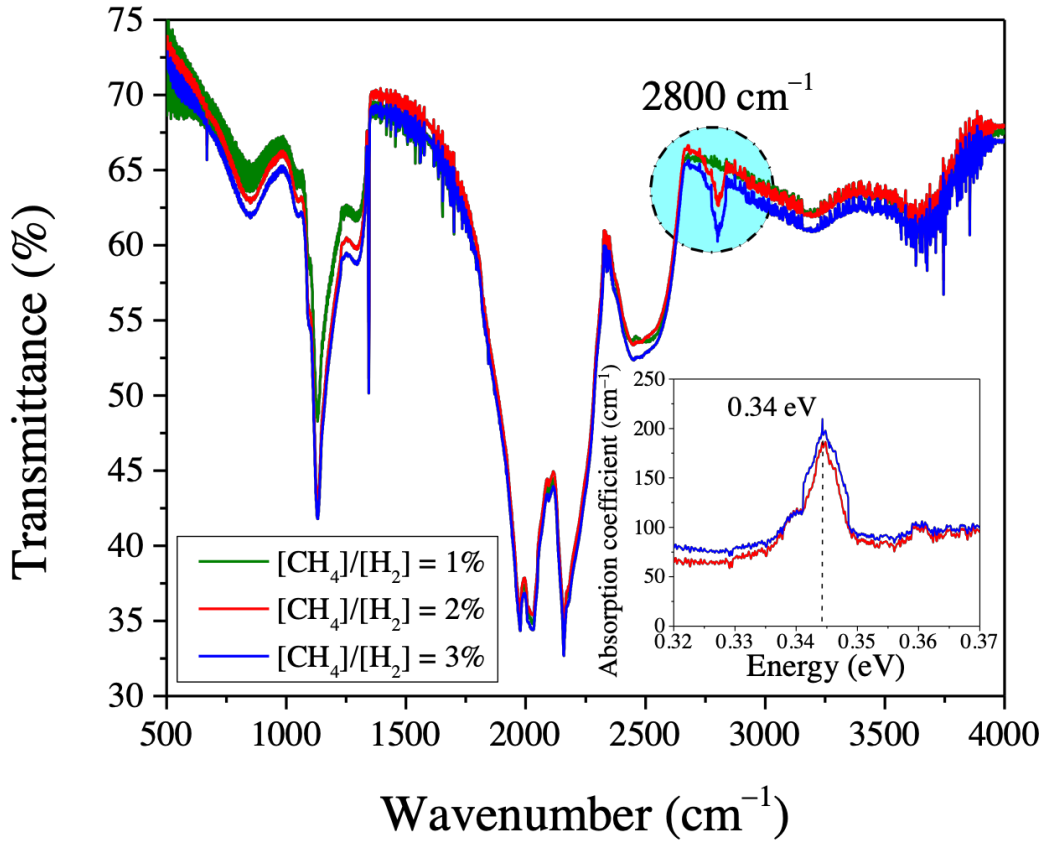

186

187 Figure 3: FTIR transmission spectra of diamond films grown at 1%, 2%, and 3% methane concentrations. The
188 inset shows the corresponding absorption coefficient vs. energy plots of the samples deposited at 2% and 3%
189 methane concentrations.

190 Figure 4 displays the details of the CL spectra (normalized with respect to the free exciton (FE)

191 at 5.27 eV) of the B-doped SCD layers grown with 1%, 2%, and 3% methane concentration in

192 the excitonic energy range at 5 K. These spectra exhibit two dominant peaks: the peak at

193 5.27 eV corresponds to the recombination of the FE assisted by a transverse optical (TO)

194 phonon (FE^{TO}), and the peak at 5.22 eV corresponds to the neutral-boron bound exciton (BE),

195 also assisted by a TO phonon (BE^{TO}). The boron acceptor concentration was calculated from

196 the ratio between the BE^{TO} and FE^{TO} recombination intensities, as given in Eq. (2):[43]

$$[B] = 3.5 \times 10^{16} \frac{I_{\mathrm{BE^{TO}}}}{I_{\mathrm{FE^{TO}}}} \ (\mathrm{cm}^{-3}) \tag{2}$$

To ensure the collection of CL signals are from the CVD grown layer, the sample deposited at 1% methane concentration was additionally measured at 10 and 20 kV (not shown here). The ratio between BE^{TO} and FE^{TO} intensities showed consistency with that measured at 30 kV, confirming that the acquired signal indeed mostly originated from the CVD doped layer. The boron content in diamond samples was found to be 5×10^{15}, 1×10^{16}, 2×10^{17} cm^{-3} for the samples grown at 1%, 2%, and 3% of methane concentrations, respectively.

The full width at half maximum (FWHM) of the FE^{TO} peak is directly related to the crystalline quality of the film.[44] The lower the defect density, the lower is the FWHM of FE^{TO} peak.[44] The samples grown at 1% and 2% methane concentrations exhibit narrower peaks (FWHM ≈ 10 meV) of the FE^{TO} peak than the sample grown with 3% methane concentration (FWHM ≈ 15 meV). This is explained by the presence of unepitaxial crystallites and pyramidal hillock defects observed on this sample by optical micrographs and AFM measurements, causing the degradation of crystalline quality.

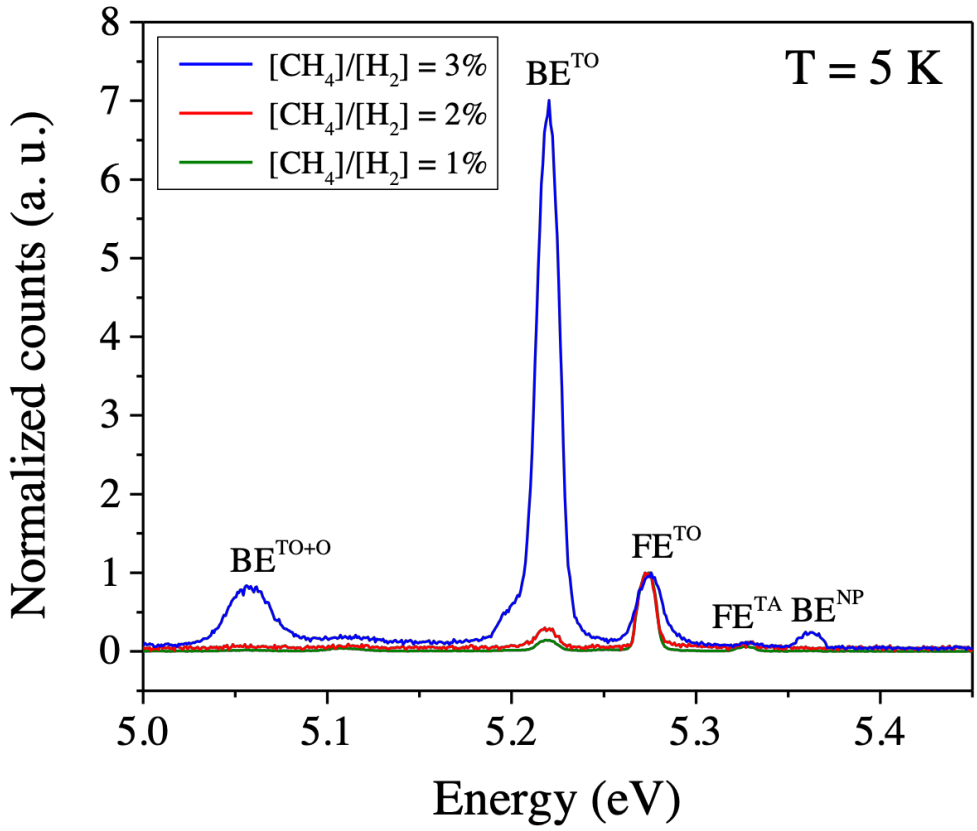

Figure 4: CL spectra of B-doped SCD films grown at 1%, 2%, and 3% methane concentrations.

The energy and FWHM of the BE^{TO} exciton show good agreement with the results achieved by other studies (Fig. 5).[44–47] In all three samples of this work, the peak position of BE^{TO} peak is neither red- nor blue-shifted from its position reported in the literature.[44] This indicates that there is no residual strain in the samples that could be caused by interstitial boron atoms in the diamond lattice structure. In the work of Ghodbane *et al.*,[44] a downward shift (0.033 eV) of the peak position of the BE^{TO} peak was reported for the B-doped SCD sample with a boron concentration of 6.2×10^{17} cm^{-3}, whereas the sample with a boron content of 3.3×10^{15} cm^{-3} showed no shift. Another possible reason for this shift would be the formation of the boron impurities energy level and the narrowing of the diamond bandgap. Here, this origin is ruled out as the boron concentration of the samples in this work is estimated to be below the minimum limitation of formation of this impurity level in diamond (1.5×10^{19} cm^{-3}).[48] The

FWHM of the BE^{TO} peak remains very low reflecting a low density of imperfections in the lattice structure of the films.

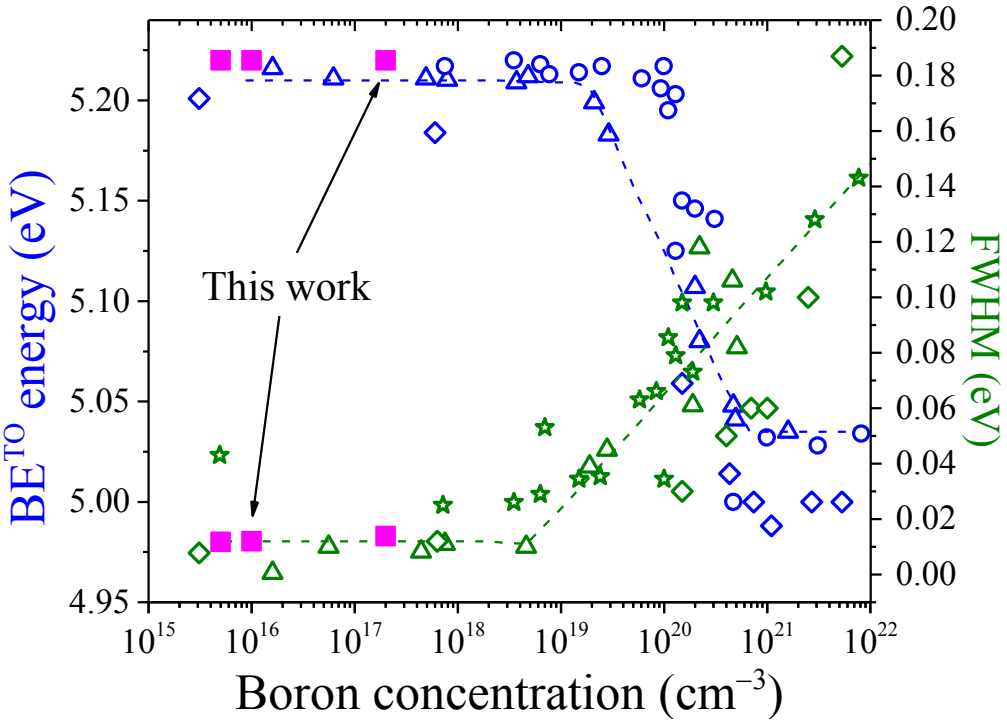

Figure 5: Peak position and FWHM of BE^{TO} as a function of boron concentration for B-doped SCD films of this study compared with previous results reported in literature: ◊—Ref. (44), Δ—Ref. (45), ○—Ref. (46), ☆— Ref. (47), and ■— this work.

Figure 6 shows the temperature dependence of electrical conductivity and hole mobility as determined by the Hall effect. All the samples showed *p*-type conductivity, which indicated that holes are the majority carriers in the films. The electrical conductivity increased with increasing temperature in all the samples, which is typical for semiconductors (Fig. 6(a)). The increase in methane concentration from 1% to 3% in the plasma feedgas resulted in the higher electrical conductivity of samples, from 15 $m\Omega^{-1}\cdot cm^{-1}$ to 0.74 $\Omega^{-1}\cdot cm^{-1}$ at room temperature, respectively. This correlates with the increase of acceptor concentration, as seen in CL and FTIR results. For B-doped SCD films grown at 1%, 2%, and 3% methane concentrations, the hole concentrations measured by Hall effect at room temperature were 8×10^{13}, 3×10^{14}, and 6×10^{15} cm^{-3}, respectively.

The hole mobility decreased with increasing the methane concentration, as shown in Figure 6(b). B-doped SCD grown at 1% methane concentration reaches a Hall mobility of (1200 ± 140) $cm^2/V\cdot s$ at 300 K, which corresponds to the higher range of the experimental values reported in boron doped layers.[15,49,50] Such a high value of Hall mobility can be attributed to the low degree of compensation and good crystalline quality of this sample.[51] Samples grown with a methane concentration of 2% and 3%, exhibit lower values of (1020 ± 130) $cm^2/V\cdot s$ and (770 ± 54) $cm^2/V\cdot s$ at room temperature, respectively. For these two B-doped SCD samples, the Hall mobility values were relatively smaller in the lower temperature range below 200 K (Fig. 6(b) inset), and decreased with increasing temperature above 500 K. The observed rapid increase in the Hall mobility of the samples grown at 2% and 3% methane concentration with temperature from 90 K to 200 K can be attributed to the contribution of hopping conduction, which has been reported in the other studies extensively.[15,52–54] Tsukioka *et al.*[52] showed that if the Hall coefficient, calculated by $K_s = \mu/\sigma$, decreases due to the effect of hopping conduction, mobility also decreases proportionally to K_s.

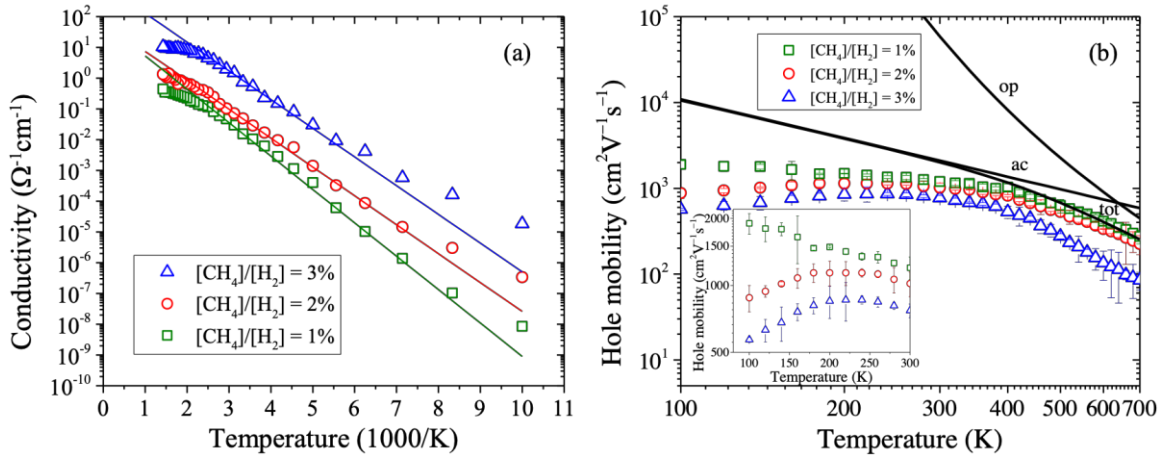

Figure 6: Temperature dependence of (a) bulk electrical conductivity and (b) hole mobility of B-doped SCD samples grown with 1%, 2%, and 3% methane concentration in the plasma feedgas. (a) The solid lines are the exponential fitting data.[53] The disparities between the fitting and experimental data at low temperatures are attributed to the hopping mechanism. (b) The solid lines show the theoretical contribution of optical phonon (op) and acoustic phonon (ac) scattering modes and the total mobility (tot), calculated from Ref. (51). Ionized and neutral impurity scattering are not included here. According to Ref. (51), their contribution at elevated temperatures (above 400 K) is considered negligible, whereas at lower temperatures (below 400 K), the data lacks the reliability necessary for fitting. The inset shows a zoom-in perspective of temperature (plotted in a linear scale) dependence of hole mobility of samples below 300 K.

The scattering mechanisms of B-doped SCD samples in Figure 6(b) were deduced from mobility temperature dependence using the model, explained in details in Ref. (51). The calculations took into account acoustic phonon (ac), and optical phonon (op) scattering mechanisms (Fig. 6(b)). In these calculations, both acoustic phonon (ac) and optical phonon (op) scattering are intrinsic to diamond and hence are assumed to be the same for all samples.[51] Once the temperature is below 400 K, the hopping mechanism assumes control over hole mobility, as discussed above, rendering fitting impossible below this temperature range. In addition, the hole mobility as a function of doping level of this study shows a good agreement with the summation of the theoretical contribution of various scattering modes,[51] together with the results of previous studies, as shown in Figure 7.[50,52,55–59]

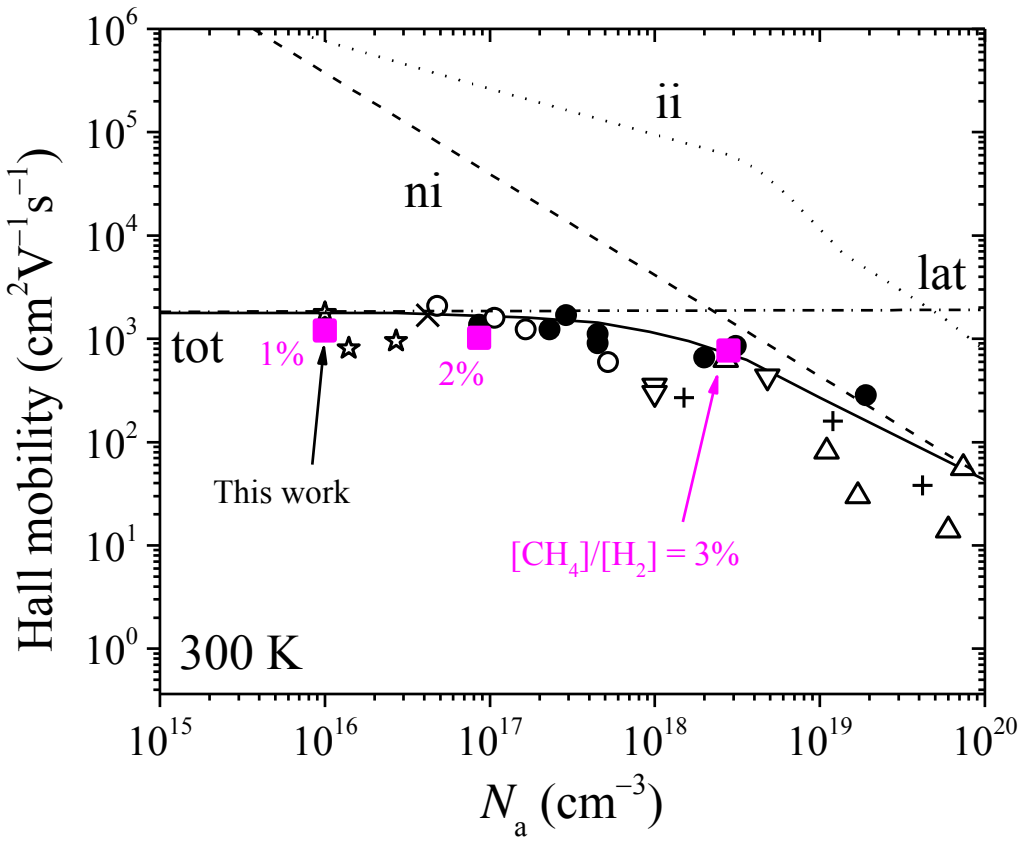

Figure 7: Room temperature Hall hole mobility as a function of N_a, calculated from Eq. (3), for lightly doped SCD films of this study compared with previous results reported in literature: +—Ref. (55), ☆—Ref. (50), ∇—Ref. (56), Δ—Ref. (57), •—Ref. (52), ○—Ref. (58), and ×—Ref. (59). The theoretical contribution of various scattering modes is illustrated by dashed and dotted line for lattice (lat), dotted line for ionized impurities (ii) mode, dashed line for neutral impurities (ni) mode, and solid line for their combination (tot).[51]

The temperature dependence of free hole concentration, $p(T)$, was fitted using neutrality equation:[60]

$$\frac{p(p+N_d)}{(N_a - N_d - p)} = \frac{N_v}{g_a}\exp\left(-\frac{E_a}{k_B T}\right) \tag{3}$$

where N_a and E_a are the density and activation energy of the acceptor, respectively, N_d is the density of compensating donors, N_v is the density of states in the valence band, k_B is the Boltzmann's constant, T is the absolute temperature, and g_a is the ground-state degeneracy factor for acceptor level. Taking into the account the spin-orbit coupling in diamond, the following expression for the degeneracy factor can be used:[56,61]

$$g_a = 4 + 2\exp\left(-\frac{\Delta}{k_B T}\right) \quad (4)$$

with Δ = 6 meV the split off by the energy as experimentally determined.[51] In these calculations, the total density-of-state mass (m^*) was taken as $0.919m_0$,[51,62] with m_0 the free electron mass. Figure 8 shows the variation of the hole concentration in the grown diamond films as a function of temperature.

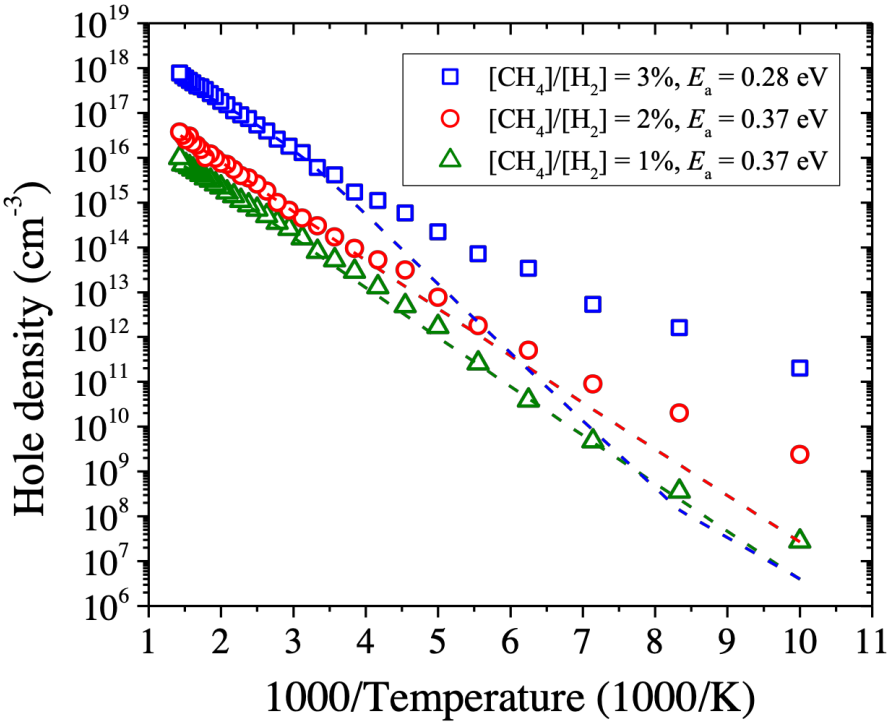

Figure 8: Hole density as a function of temperature of the B-doped diamond layers grown at different methane concentrations. The fitting data calculated by using Eq. (3), are plotted as the dashed lines.

The results of the hole concentration fitting by the neutrality equation (Eq. (3)) are presented in Table 1. These findings align with the results obtained through other methods (FTIR and CL spectroscopy), which also demonstrated that an elevated methane concentration in the CVD plasma corresponds to an increased level of boron incorporation in the grown layers. During the fitting process, the domination of hopping conduction at low temperatures hinders reliable estimation of compensation based on hole density data, and therefore there is deficiency in

available data for fitting. Nonetheless, based on the fitting variability on the available reliable data, the compensation ratio of the sample is assumed to be no higher than 7%.

XPS measurements were carried out to evaluate and compare the boron content of the surface bonds of the B-doped SCD films of this study, and to investigate the C 1s core level components and their change with B-doping. The XPS B1s spectra from the surface of the samples are shown in Figure 9. The peak at ≈ 188.5 eV is assigned to a bond of boron at a substitutional position with carbon in the diamond lattice.[63–65] The intensity of this peak drastically increased with increasing the methane concentration from 2% to 3% in plasma feedgas. This peak was not observed in the sample grown at 1% methane concentration. The presence of B1s peak at ≈ 188.5 eV has been mostly reported in heavily B-doped diamond films (≥ 10^{20} cm^{-3}).[64–66]

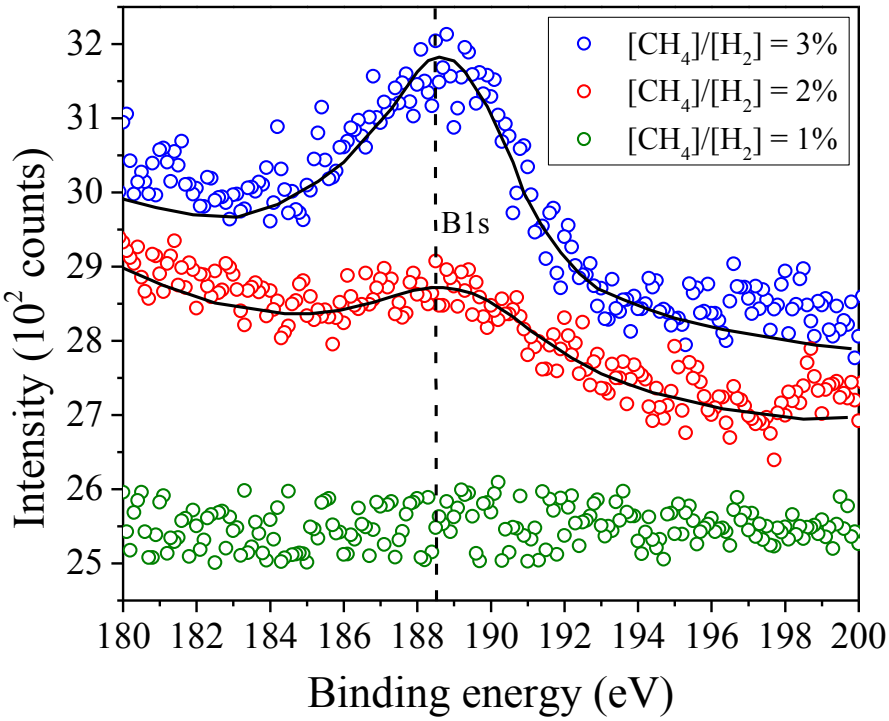

Figure 9: The XPS B1s spectra of B-doped SCD films grown at 1%, 2%, and 3% methane concentrations in the plasma feedgas.

Figure 10 shows the C1s core level spectra of the films grown with 1%, 2%, and 3% methane concentration in the plasma feedgas. The C1s peaks are centered on ≈ 284 eV in all the films.

318 A slight widening of the C1s is observed as the methane concentration increases. The FWHM
319 of C1s peak increased from 0.59 eV to 0.88 eV by increasing the methane concentration from
320 1% to 3% in the plasma. Ghodbane *et al.*[67,68] reported the same broadening of C1s peak by
321 increasing the boron incorporation in their samples. This widening of the C1s peak is also
322 accompanied by an increase of its components' intensities mostly at the higher energy side.
323 This is particularly visible for the sample grown with 3% methane concentration, as shown in
324 the inset of Figure 10. The main component is attributed to the carbon σ bond (C−C) core level
325 of diamond surface.[67,69,70] The second important component is associated to CH_x bounds with
326 (x = 2 or 3), which results from carbon-hydrogen bounds at the diamond surface and
327 subsurface.[67,69,70] Two oxygenated groups (C−O−C and >C=O) were also found in the
328 samples.[68,70] The component at 282.4 eV is usually referred to the carbon double bond (C=C)
329 and can be assigned to the residual dimers at the diamond surface.[67,68]

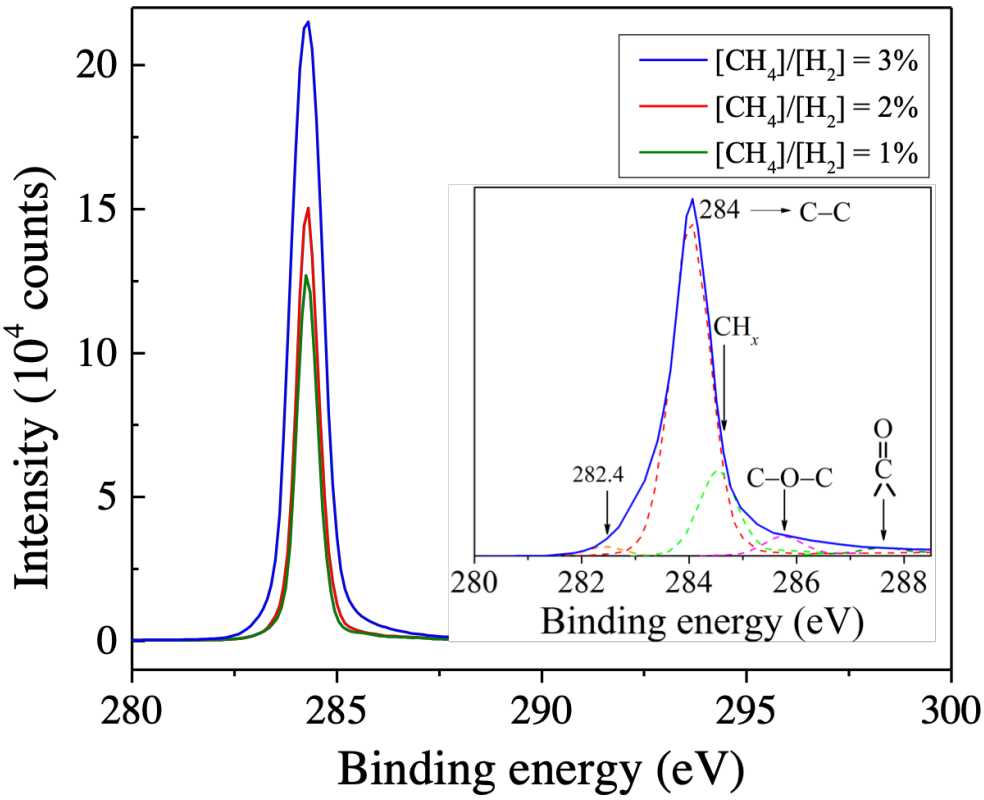

Figure 10: The XPS C1s spectra of B-doped SCD films grown at 1%, 2%, and 3% methane concentrations in the plasma feedgas. The inset shows the fit of the C1s energy range for the sample grown at 3% methane concentration.

Finally, Figure 11 illustrates the evaluation of concentration of C−C and CH_x ($x = 2$ or 3) groups as a function of boron concentration determined by CL spectroscopy, and compares it with other studies.[67,68] In the low doping range, where the samples of this study are located, the C-C concentration decreases with increasing [B] concentration while that of CH_x group increases. The increase of CH_x concentrations might be ascribed to the increase of C−C bond length occurring when there is higher [B] concentration, as described by Ghodbane *et al.*[68]

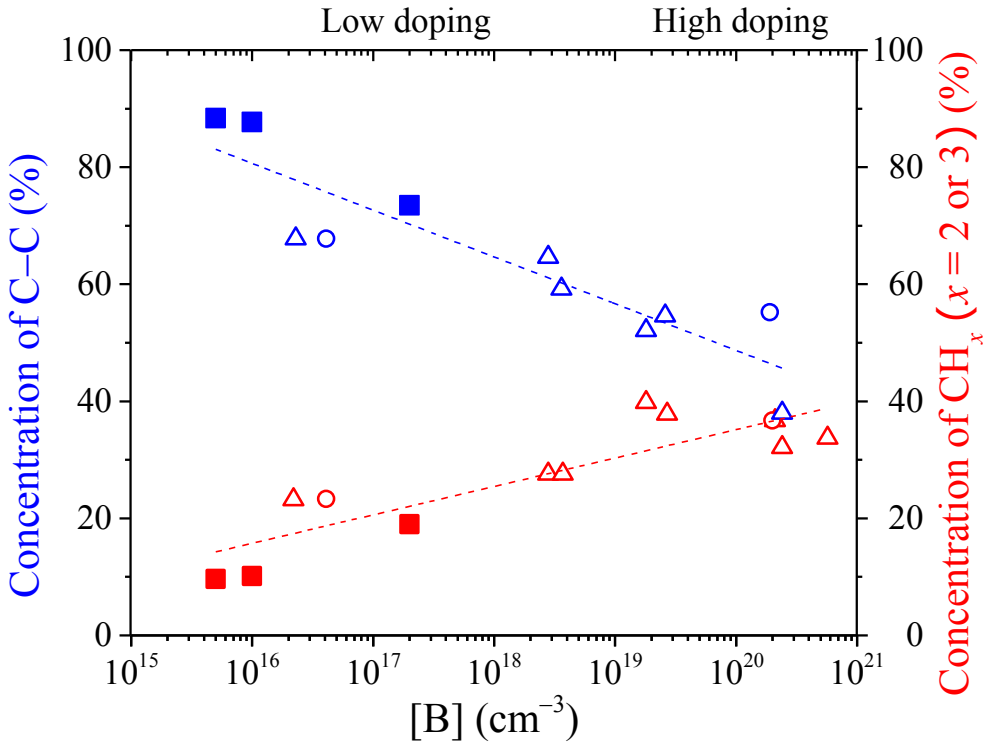

Figure 11: Comparisons of the concentrations of C−C and CH_x (x = 2 or 3) according to the boron concentration with previous results reported in the literature: ○—Ref. (67), Δ—Ref. (68), and ■ —this study.

The XPS results are in reasonable agreement with the FTIR, CL, and Hall effect results shown in Table 1, revealing a strong positive correlation of the boron level with the methane concentration in the plasma feedgas, that is, higher methane concentrations lead to higher boron content. Moreover, as the growth with 3% methane concentration was performed as the last and no intentional boron-containing gas precursor added, a reduced boron concentration in the deposition chamber can be ruled out.

The variation in boron concentration determined by different techniques is an issue, which has been also previously reported by other research groups, like Demlow *et al.*[71] that shows the overestimation of boron content calculated by FTIR compared to the result of secondary ions mass spectroscopy, due to the imperfect transmission through the grown samples and/or the presence of defects such as dark colored unepitaxial defects in FTIR spectroscopy. The

inhomogeneity of the boron concentration in the CVD grown layers may also be one possible cause of the variation in the measured boron content by different methods.

Table 1: Summary of the doping concentrations of samples measured by different techniques.

$[CH_4]/[H_2]$ (%)	Growth rate at sample center (μm/h)	$[N_a - N_d]$ by FTIR (cm^{-3})	[B] by CL (cm^{-3})	N_a by Hall effect (cm^{-3})
1	1[§]	-[‡]	5×10^{15}	$(1.0 \pm 0.5) \times 10^{16}$
2	2.1 ± 0.1[†]	4.5×10^{17}	1×10^{16}	$(8.6 \pm 1.0) \times 10^{16}$
3	2.8 ± 0.1[†]	5.6×10^{17}	2×10^{17}	$(2.8 \pm 0.7) \times 10^{18}$

§ - Determined via transmission electron microscopy.

‡ - No measurable data.

† - Measured by Mitutoyo linear gage.

Conclusions

Unintentionally boron doped SCD (100)-oriented films were deposited by MW PE CVD using a $[CH_4]/[H_2]$ range from 1% to 3% in the plasma feedgas. For the samples grown at 1% and 2% methane concentrations, a high surface quality was observed by means of a low density of surface defects. With increasing the methane concentration to 3%, the appearance of superficial defects on the grown diamond layers as well as the increase of the FWHM free-exciton FE^{TO} peak in the CL spectra were observed, most likely due to the higher growth rate. The electrical conductivity of samples increased from 15 $m\Omega^{-1}\cdot cm^{-1}$ to 0.74 $\Omega^{-1}\cdot cm^{-1}$ at room temperature with increasing the methane concentration from 1% to 3% in the plasma feedgas. The hopping conduction mechanism at low temperatures ($90\ K \leq T \leq 200\ K$) was discussed by the electrical conductivity, mobility, and hole concentration results. The mobility analysis shows the dominant role of acoustic phonon (ac) and optical phonon (op) scattering mechanisms for all used methane concentrations samples. In addition, the doping dependence of the Hall hole mobility of this study showed a good agreement with the calculations and the previously reported results. The results of FTIR, CL, Hall effect, and XPS measurements showed that by

increasing the methane concentration, the B-doping level increased. This study sheds light on the important role of methane concentration in controlling the B-doping levels of lightly *p*-type SCD films, a *sine qua non* requirement for the fabrication of high power electronic applications and low concentration colour center creation.

Acknowledgments

The Research Foundation – Flanders (FWO) is gratefully acknowledged for financial support in the form of projects S004018N, and G0D4920N, as is the Methusalem NANO network. Part of the research leading to these results has been performed within the Tournesol project funded by the FWO under grant agreement VS00822N. The authors acknowledge the support of the staff members, Dr. Christian Schulz and Dr. Tristan Petit, at BESSY II Synchrotron Research Facility.

References

(1) *Green Diamond*. Green electronics with diamond power Devices. [Online, **2024**]: https://www.greendiamond-project.eu.

(2) Wang, R.; Peng, B.; Bai, H.; Guo, Z.; Wei, Q.; Wang, K.; Yu, C.; Niu, G.; Wang, H.-X. Morphology, Defects and Electrical Properties of Boron-Doped Single Crystal Diamond under Various Oxygen Concentration. *Mater. Lett.* **2022**, *322*, 132345. https://doi.org/10.1016/j.matlet.2022.132345.

(3) *Diamond Power Transistors*. [Online, **2024**]: https://arpa-e.energy.gov/technologies/projects/diamond-power-transistors.

(4) *Development of diamond power electronics*. [Online, **2024**]: https://kaken.nii.ac.jp/en/grant/KAKENHI-PROJECT-18KK0383/.

(5) Wang, Z.; Liu, Y.; Zhao, H.; Li, B.; Guo, Q.; Ma, H.; Jia, X. Boron-Doped Diamond Growth and Characteristics in a Ni-Based Alloy Catalyst System at HPHT Conditions. *Int. J. Refract. Met. Hard Mater.* **2023**, *117*, 106404. https://doi.org/10.1016/j.ijrmhm.2023.106404.

(6) Solomnikova, A.; Lukashkin, V.; Zubkov, V.; Kuznetsov, A.; Solomonov, A. Carrier Concentration Variety over Multisectoral Boron-Doped HPHT Diamond. *Semicond. Sci. Technol.* **2020**, *35* (9), 095005. https://doi.org/10.1088/1361-6641/ab9a5f.

(7) Strelchuk, V. V.; Nikolenko, A. S.; Lytvyn, P. M.; Ivakhnenko, S. O.; Kovalenko, T. V.; Danylenko, I. M.; Malyuta, S. V. Growth-Sector Dependence of Morphological, Structural and Optical Features in Boron-Doped HPHT Diamond Crystals. *Semicond. Physics, Quantum Electron. Optoelectron.* **2021**, *24* (3), 261–271. https://doi.org/10.15407/spqeo24.03.261.

(8) Issaoui, R.; Achard, J.; William, L.; Mehmel, L.; Pinault Thaury, M. A.; Bénédic, F. Thick and Widened High Quality Heavily Boron Doped Diamond Single Crystals Synthetized with High Oxygen Flow under High Microwave Power Regime. *Diam. Relat. Mater.* **2019**, *94* (November 2018), 88–91. https://doi.org/10.1016/j.diamond.2019.03.001.

(9) Umezawa, H.; Kato, Y.; Shikata, S. 1 Ω On-Resistance Diamond Vertical-Schottky Barrier Diode Operated at 250°C. *Appl. Phys. Express* **2013**, *6* (1), 011302. https://doi.org/10.7567/APEX.6.011302.

(10) Volpe, P.-N.; Muret, P.; Pernot, J.; Omnès, F.; Teraji, T.; Jomard, F.; Planson, D.; Brosselard, P.; Dheilly, N.; Vergne, B.; Scharnholtz, S. High Breakdown Voltage Schottky Diodes Synthesized on P-Type CVD Diamond Layer. *Phys. status solidi* **2010**, *207* (9), 2088–2092. https://doi.org/10.1002/pssa.201000055.

(11) Kobayashi, A.; Ohmagari, S.; Umezawa, H.; Takeuchi, D.; Saito, T. Suppression of Killer Defects in Diamond Vertical-Type Schottky Barrier Diodes. *Jpn. J. Appl. Phys.* **2020**, *59*, SGGD10. https://doi.org/10.7567/1347-4065/ab65b1.

(12) Donato, N.; Rouger, N.; Pernot, J.; Longobardi, G.; Udrea, F. Diamond Power Devices: State of the Art, Modelling, Figures of Merit and Future Perspective. *J. Phys. D. Appl. Phys.* **2020**, *53* (9), 093001. https://doi.org/10.1088/1361-6463/ab4eab.

(13) Nemanich, R. J.; Carlisle, J. A.; Hirata, A.; Haenen, K. CVD Diamond—Research, Applications, and Challenges. *MRS Bull.* **2014**, *39* (6), 490–494. https://doi.org/10.1557/mrs.2014.97.

(14) Seki, Y.; Hoshino, Y.; Nakata, J. Extremely High-Efficient Activation of Acceptor Boron Introduced by Ion Implantation at Room Temperature with Various Doping Concentrations in Epitaxially Synthesized Diamond Films by Chemical Vapor Deposition. *J. Appl. Phys.* **2021**, *129* (19), 195702. https://doi.org/10.1063/5.0048309.

(15) Barjon, J.; Chikoidze, E.; Jomard, F.; Dumont, Y.; Pinault-Thaury, M. A.; Issaoui, R.; Brinza, O.; Achard, J.; Silva, F. Homoepitaxial Boron-Doped Diamond with Very Low Compensation. *Phys. Status Solidi Appl. Mater. Sci.* **2012**, *209* (9), 1750–1753. https://doi.org/10.1002/pssa.201200136.

(16) Ohmagari, S.; Yamada, H.; Tsubouchi, N.; Umezawa, H.; Chayahara, A.; Seki, A.; Kawaii, F.; Saitoh, H.; Mokuno, Y. Schottky Barrier Diodes Fabricated on Diamond Mosaic Wafers: Dislocation Reduction to Mitigate the Effect of Coalescence Boundaries. *Appl. Phys. Lett.* **2019**, *114* (8), 082104. https://doi.org/10.1063/1.5085364.

(17) Arnault, J.-C.; Saada, S.; Ralchenko, V. Chemical Vapor Deposition Single-Crystal Diamond: A Review. *Phys. status solidi – Rapid Res. Lett.* **2022**, *16* (1), 2100354.

https://doi.org/10.1002/pssr.202100354.

(18) Lloret, F.; Araujo, D.; Eon, D.; del Pilar Villar, M.; Gonzalez-Leal, J. M.; Bustarret, E. Influence of Methane Concentration on MPCVD Overgrowth of 100-Oriented Etched Diamond Substrates. *Phys. Status Solidi A.* **2016**, *213* (10), 2570–2574. https://doi.org/10.1002/pssa.201600182.

(19) Widmann, C. J.; Hetzl, M.; Drieschner, S.; Nebel, C. E. Homoepitaxial Growth of High Quality (111)-Oriented Single Crystalline Diamond. *Diam. Relat. Mater.* **2017**, *72*, 41–46. https://doi.org/10.1016/j.diamond.2016.12.020.

(20) Zhang, P.; Chen, W.; Zhang, L.; He, S.; Wang, H.; Yan, S.; Ma, W.; Guo, C.; Wang, Y. Evolution of High-Quality Homoepitaxial CVD Diamond Films Induced by Methane Concentration. *Coatings* **2021**, *11* (8), 888. https://doi.org/10.3390/coatings11080888.

(21) Lloret, F.; Soto, B.; Rouzbahani, R.; Gutiérrez, M.; Haenen, K.; Araujo, D. High Phosphorous Incorporation in (100)-Oriented MP CVD Diamond Growth. *Diam. Relat. Mater.* **2023**, *133*, 109746. https://doi.org/10.1016/j.diamond.2023.109746.

(22) Takeuchi, D.; Yamanaka, S.; Watanabe, H.; Sawada, S.; Ichinose, H.; Okushi, H.; Kajimura, K. High Quality Homoepitaxial Diamond Thin Film Synthesis with High Growth Rate by a Two-Step Growth Method. *Diam. Relat. Mater.* **1999**, *8* (6), 1046–1049. https://doi.org/10.1016/S0925-9635(99)00002-3.

(23) Rouzbahani, R.; Nicley, S. S.; Vanpoucke, D. E. P.; Lloret, F.; Pobedinskas, P.; Araujo, D.; Haenen, K. Impact of Methane Concentration on Surface Morphology and Boron Incorporation of Heavily Boron-Doped Single Crystal Diamond Layers. *Carbon N. Y.* **2021**, *172*, 463–473. https://doi.org/10.1016/j.carbon.2020.10.061.

(24) Alegre, M. P.; Araújo, D.; Fiori, A.; Pinero, J. C.; Lloret, F.; Villar, M. P.; Achatz, P.;

Chicot, G.; Bustarret, E.; Jomard, F. Critical Boron-Doping Levels for Generation of Dislocations in Synthetic Diamond. *Appl. Phys. Lett.* **2014**, *105* (17), 173103. https://doi.org/10.1063/1.4900741.

(25) Teraji, T.; Ito, T. Homoepitaxial Diamond Growth by High-Power Microwave-Plasma Chemical Vapor Deposition. *J. Cryst. Growth* **2004**, *271* (3–4), 409–419. https://doi.org/10.1016/j.jcrysgro.2004.08.005.

(26) Umezawa, H.; Tatsumi, N.; Kato, Y.; Shikata, S. I. Leakage Current Analysis of Diamond Schottky Barrier Diodes by Defect Imaging. *Diam. Relat. Mater.* **2013**, *40*, 56–59. https://doi.org/10.1016/j.diamond.2013.09.011.

(27) Ohmagari, S.; Yamada, H.; Tsubouchi, N.; Umezawa, H.; Chayahara, A.; Tanaka, S.; Mokuno, Y. Large Reduction of Threading Dislocations in Diamond by Hot-Filament Chemical Vapor Deposition Accompanying W Incorporations. *Appl. Phys. Lett.* **2018**, *113* (3), 032108. https://doi.org/10.1063/1.5040658.

(28) Achard, J.; Jacques, V.; Tallaire, A. CVD Diamond Single Crystals with NV Centres: A Review of Material Synthesis and Technology for Quantum Sensing Applications. *J. Phys. D. Appl. Phys.* **2020**, *53* (31), 313001. https://doi.org/10.1088/1361-6463/ab81d1.

(29) Rouzbahani, R. Heavily Boron-Doped CVD Diamond for Pseudo-Vertical Schottky Barrier Diodes, Doctoral Dissertation, Hasselt University, **2021**. https://anet.be/record/uhasseltopacdt/c:lvd:15308745/N.

(30) Mortet, V.; Pernot, J.; Jomard, F.; Soltani, A.; Remes, Z.; Barjon, J.; D'Haen, J.; Haenen, K. Properties of Boron-Doped Epitaxial Diamond Layers Grown on (110) Oriented Single Crystal Substrates. *Diam. Relat. Mater.* **2015**, *53*, 29–34. https://doi.org/10.1016/j.diamond.2015.01.006.

(31) Schulz, C.; Lieutenant, K.; Xiao, J.; Hofmann, T.; Wong, D.; Habicht, K. Characterization of the Soft X-Ray Spectrometer PEAXIS at BESSY II. **2020**, *27*, 238–249. https://doi.org/10.1107/S1600577519014887.

(32) SPECS. *Phoibos 150 Nap*. [Online, **2024**]: http://www.specs.de/cms/front_content.php?idcat=269%0Ahttp://www.specs.de/cms/upload/PDFs/SPECS_Prospekte/2010_11_PHOIBOS_150_NAP_product_brochure_final_web.pdf.

(33) Lloret, F.; Eon, D.; Bustarret, E.; Araujo, D. Crystalline Defects Induced during MPCVD Lateral Homoepitaxial Diamond Growth. *Nanomaterials* **2018**, *8* (10), 60-65. https://doi.org/10.3390/nano8100814.

(34) Smallman, R. E.; Bishop, R. J. Defects in Solids. In *Modern Physical Metallurgy and Materials Engineering*; Elsevier, **1999**, 84–124. https://doi.org/10.1016/b978-075064564-5/50004-5.

(35) Ashkinazi, E.; Khmelnitskii, R.; Sedov, V.; Khomich, A.; Khomich, A.; Ralchenko, V. Morphology of Diamond Layers Grown on Different Facets of Single Crystal Diamond Substrates by a Microwave Plasma CVD in CH_4-H_2-N_2 Gas Mixtures. *Crystals* **2017**, *7* (6), 166. https://doi.org/10.3390/cryst7060166.

(36) Tallaire, A.; Kasu, M.; Ueda, K.; Makimoto, T. Origin of Growth Defects in CVD Diamond Epitaxial Films. *Diam. Relat. Mater.* **2008**, *17* (1), 60–65. https://doi.org/10.1016/j.diamond.2007.10.003.

(37) Tarutani, M.; Takai, Y.; Shimizu, R.; Ando, T.; Kamo, M.; Bando, Y. Transmission Electron Microscopy Study of Interface and Internal Defect Structures of Homoepitaxial Diamond. *Appl. Phys. Lett.* **1996**, *68* (15), 2070–2072. https://doi.org/10.1063/1.116306.

(38) Fernández-Lorenzo, C.; Araújo, D.; González-Mañas, M.; Martín, J.; Navas, J.; Alcántara, R.; Villar, M. P.; Bagriantsev, D. Multi-Technique Analysis of High Quality HPHT Diamond Crystal. *J. Cryst. Growth* **2012**, *353* (1), 115–119. https://doi.org/10.1016/j.jcrysgro.2012.05.007.

(39) Chevallier, J.; Lusson, A.; Ballutaud, D.; Theys, B.; Jomard, F.; Deneuville, A.; Bernard, M.; Gheeraert, E.; Bustarret, E. Hydrogen-Acceptor Interactions in Diamond. *Diam. Relat. Mater.* **2001**, *10* (3–7), 399–404. https://doi.org/10.1016/S0925-9635(00)00432-5.

(40) Gheeraert, E.; Deneuville, A.; Mambou, J. Boron-Related Infra-Red Absorption in Homoepitaxial Diamond Films. *Diam. Relat. Mater.* **1998**, *7* (10), 1509–1512. https://doi.org/10.1016/S0925-9635(98)00223-4.

(41) Demlow, S. N. N.; Grotjohn, T. A. A.; Hogan, T.; Becker, M.; Asmussen, J. Determination of Boron Concentration in Doped Diamond Films. *MRS Proc.* **2011**, *1282*, mrsf10-1282-a05-15. https://doi.org/10.1557/opl.2011.444.

(42) Collins, A. T.; Williams, A. W. S. The Nature of the Acceptor Centre in Semiconducting Diamond. *J. Phys. C Solid State Phys.* **1971**, *4* (13), 1789–1800. https://doi.org/10.1088/0022-3719/4/13/030.

(43) Omnès, F.; Muret, P.; Volpe, P. N.; Wade, M.; Pernot, J.; Jomard, F. Study of Boron Doping in MPCVD Grown Homoepitaxial Diamond Layers Based on Cathodoluminescence Spectroscopy, Secondary Ion Mass Spectroscopy and Capacitance-Voltage Measurements. *Diam. Relat. Mater.* **2011**, *20* (7), 912–916. https://doi.org/10.1016/j.diamond.2011.05.010.

(44) Ghodbane, S.; Omnès, F.; Agnès, C. A Cathodoluminescence Study of Boron Doped {111}-Homoepitaxial Diamond Films. *Diam. Relat. Mater.* **2010**, *19* (4), 273–278.

https://doi.org/10.1016/j.diamond.2009.11.003.

(45) Baron, C.; Wade, M.; Deneuville, A.; Jomard, F.; Chevallier, J. Cathodoluminescence of Highly and Heavily Boron Doped (100) Homoepitaxial Diamond Films. *Diam. Relat. Mater.* **2006**, *15* (4–8), 597–601. https://doi.org/10.1016/j.diamond.2006.01.015.

(46) Sauer, R. *Thin-Film Diamond I*; Nebel, C. E. J. R., Ed.; Semicond. Semimet., **2004**, *76*, 379. https://doi.org/10.1016/S0080-8784(03)80003-0.

(47) Sternschulte, R. S. H.; Tachibana, T.; Thonke, K. *The Physics of Semiconductor*; Scheffler, M., Zimmermann, R., Eds.; World Scientific: Singapore, **1996**.

(48) Tanabe, K.; Nakazawa, K.; Susantyo, J.; Kawarada, H.; Koizumi, S. Cathodoluminescence of Phosphorus Doped (111) Homoepitaxial Diamond Thin Films. *Diam. Relat. Mater.* **2001**, *10* (9–10), 1652–1654. https://doi.org/10.1016/S0925-9635(01)00389-2.

(49) Yap, C. M.; Ansari, K.; Xiao, S.; Yee, S. Y.; Chukka, R.; Misra, D. S. Properties of Near-Colourless Lightly Boron Doped CVD Diamond. *Diam. Relat. Mater.* **2018**, *88* (July), 118–122. https://doi.org/10.1016/j.diamond.2018.07.001.

(50) Volpe, P. N.; Pernot, J.; Muret, P.; Omnès, F. High Hole Mobility in Boron Doped Diamond for Power Device Applications. *Appl. Phys. Lett.* **2009**, *94* (9), 12–15. https://doi.org/10.1063/1.3086397.

(51) Pernot, J.; Volpe, P. N.; Omnès, F.; Muret, P.; Mortet, V.; Haenen, K.; Teraji, T. Hall Hole Mobility in Boron-Doped Homoepitaxial Diamond. *Phys. Rev. B - Condens. Matter Mater. Phys.* **2010**, *81* (20), 205203. https://doi.org/10.1103/PhysRevB.81.205203.

(52) Tsukioka, K.; Okushi, H. Hall Mobility and Scattering Mechanism of Holes in Boron-

Doped Homoepitaxial Chemical Vapor Deposition Diamond Thin Films. *Japanese J. Appl. Physics, Part 1 Regul. Pap. Short Notes Rev. Pap.* **2006**, *45* (11), 8571–8577. https://doi.org/10.1143/JJAP.45.8571.

(53) Visser, E. P.; Bauhuis, G. J.; Janssen, G.; Vollenberg, W.; Van Enckevort, J. P.; Giling, L. J. Electrical Conduction in Homoepitaxial, Boron-Doped Diamond Films. *J. Phys. Condens. Matter* **1992**, *4* (36), 7365–7376. https://doi.org/10.1088/0953-8984/4/36/011.

(54) Aono, M.; Maida, O.; Ito, T. Hall Data Analysis of Heavily Boron-Doped CVD Diamond Films Using a Model Considering an Impurity Band Well Separated from Valence Bands. *Diam. Relat. Mater.* **2011**, *20* (10), 1357–1362. https://doi.org/10.1016/j.diamond.2011.08.008.

(55) Thonke, K. The Boron Acceptor in Diamond. *Semicond. Sci. Technol.* **2003**, *18* (3), S20. https://doi.org/10.1088/0268-1242/18/3/303.

(56) Gabrysch, M.; Majdi, S.; Hallén, A.; Linnarsson, M.; Schöner, A.; Twitchen, D.; Isberg, J. Compensation in Boron-Doped CVD Diamond. *Phys. Status Solidi Appl. Mater. Sci.* **2008**, *205* (9), 2190–2194. https://doi.org/10.1002/pssa.200879711.

(57) Werner, M.; Locher, R.; Kohly, W.; Holmes, D. S.; Klose, S.; Fecht, H. J. The Diamond Irvin Curve. *Diam. Relat. Mater.* **1997**, *6* (2–4), 308–313. https://doi.org/10.1016/s0925-9635(96)00683-8.

(58) Mortet, V.; Daenen, M.; Teraji, T.; Lazea, A.; Vorlicek, V.; D'Haen, J.; Haenen, K.; D'Olieslaeger, M. Characterization of Boron Doped Diamond Epilayers Grown in a NIRIM Type Reactor. *Diam. Relat. Mater.* **2008**, *17* (7–10), 1330–1334. https://doi.org/10.1016/j.diamond.2008.01.087.

(59) Teraji, T.; Wada, H.; Yamamoto, M.; Arima, K.; Ito, T. Highly Efficient Doping of

Boron into High-Quality Homoepitaxial Diamond Films. *Diam. Relat. Mater.* **2006**, *15* (4–8), 602–606. https://doi.org/10.1016/j.diamond.2006.01.011.

(60) Pernot, J.; Contreras, S.; Camassel, J. Electrical Transport Properties of Aluminum-Implanted 4H–SiC. *J. Appl. Phys.* **2005**, *98* (2), 023706. https://doi.org/10.1063/1.1978987.

(61) Fontaine, F. Calculation of the Hole Concentration in Boron-Doped Diamond. *J. Appl. Phys.* **1999**, *85* (3), 1409–1422. https://doi.org/10.1063/1.369272.

(62) Naka, N.; Fukai, K.; Handa, Y.; Akimoto, I. Direct Measurement via Cyclotron Resonance of the Carrier Effective Masses in Pristine Diamond. *Phys. Rev. B Condens. Matter* **2013**, *88* (3), 035205. https://doi.org/10.1103/PhysRevB.88.035205.

(63) Genisel, M. F.; Uddin, M. N.; Say, Z.; Kulakci, M.; Turan, R.; Gulseren, O.; Bengu, E. Bias in Bonding Behavior among Boron, Carbon, and Nitrogen Atoms in Ion Implanted a-BN, a-BC, and Diamond like Carbon Films. *J. Appl. Phys.* **2011**, *110* (7), 074906. https://doi.org/10.1063/1.3638129.

(64) Suo, N.; Huang, H.; Wu, A.; Cao, G.; Hou, X.; Zhang, G. Porous Boron Doped Diamonds as Metal-Free Catalysts for the Oxygen Reduction Reaction in Alkaline Solution. *Appl. Surf. Sci.* **2018**, *439*, 329–335. https://doi.org/10.1016/j.apsusc.2017.12.198.

(65) Mavrin, B. N.; Denisov, V. N.; Popova, D. M.; Skryleva, E. A.; Kuznetsov, M. S.; Nosukhin, S. A.; Terentiev, S. A.; Blank, V. D. Boron Distribution in the Subsurface Region of Heavily Doped IIb Type Diamond. *Phys. Lett. Sect. A Gen. At. Solid State Phys.* **2008**, *372* (21), 3914–3918. https://doi.org/10.1016/j.physleta.2008.02.064.

(66) Hao, L.-C.; Chen, Z.-A.; Liu, D.-Y.; Zhao, W.-K.; Zhang, M.; Tang, K.; Zhu, S.-M.; Ye,

J.-D.; Zhang, R.; Zheng, Y.-D.; Gu, S.-L. Suppression and Compensation Effect of Oxygen on Heavily Boron Doping Behavior in Diamond Films. *Chinese Phys. B* **2023**, *32* (3), 038101. https://doi.org/10.1088/1674-1056/ac7f8a.

(67) Ghodbane, S.; Ballutaud, D.; Omnès, F.; Agnès, C. Comparison of the XPS Spectra from Homoepitaxial {111}, {100} and Polycrystalline Boron-Doped Diamond Films. *Diam. Relat. Mater.* **2010**, *19* (5–6), 630–636. https://doi.org/10.1016/j.diamond.2010.01.014.

(68) Ghodbane, S.; Ballutaud, D.; Deneuville, A.; Baron, C. Influence of Boron Concentration on the XPS Spectra of the (100) Surface of Homoepitaxial Boron-Doped Diamond Films. *Phys. Status Solidi Appl. Mater. Sci.* **2006**, *203* (12), 3147–3151. https://doi.org/10.1002/pssa.200671123.

(69) Graupner, R.; Maier, F.; Ristein, J.; Ley, L.; Jung, C. High-Resolution Surface-Sensitive C Core-Level Spectra of Clean and Hydrogen-Terminated Diamond (100) and (111) Surfaces. *Phys. Rev. B - Condens. Matter Mater. Phys.* **1998**, *57* (19), 12397–12409. https://doi.org/10.1103/PhysRevB.57.12397.

(70) Ferro, S.; Dal Colle, M.; De Battisti, A. Chemical Surface Characterization of Electrochemically and Thermally Oxidized Boron-Doped Diamond Film Electrodes. *Carbon N. Y.* **2005**, *43* (6), 1191–1203. https://doi.org/10.1016/j.carbon.2004.12.012.

(71) Demlow, S. N.; Rechenberg, R.; Grotjohn, T. The Effect of Substrate Temperature and Growth Rate on the Doping Efficiency of Single Crystal Boron Doped Diamond. *Diam. Relat. Mater.* **2014**, *49*, 19–24. https://doi.org/10.1016/j.diamond.2014.06.006.